PAPER • OPEN ACCESS

Gapless spin liquid and pair density wave of the Hubbard model on three-leg triangular cylinders

New Journal of Physics
The open access journal at the forefront of physics

Deutsche Physikalische Gesellschaft DPG
IOP Institute of Physics

Published in partnership with: Deutsche Physikalische Gesellschaft and the Institute of Physics

OPEN ACCESS

RECEIVED
21 September 2021

REVISED
10 November 2021

ACCEPTED FOR PUBLICATION
16 November 2021

PUBLISHED
2 December 2021

PAPER

Gapless spin liquid and pair density wave of the Hubbard model on three-leg triangular cylinders

Cheng Peng[1], **Yi-Fan Jiang**[1], **Yao Wang**[2] and **Hong-Chen Jiang**[1,*]

[1] Stanford Institute for Materials and Energy Sciences, SLAC National Accelerator Laboratory and Stanford University, Menlo Park, CA 94025, United States of America
[2] Department of Physics and Astronomy, Clemson University, Clemson, SC 29631, United States of America
[*] Author to whom any correspondence should be addressed.

E-mail: hcjiang@stanford.edu

Keywords: Hubbard model, spin liquid, doping spin liquid, superconductivity, pair density wave, triangular lattice, DMRG

Supplementary material for this article is available online

Abstract

We study the ground state properties of the Hubbard model on three-leg triangular cylinders using large-scale density-matrix renormalization group simulations. At half-filling, we identify an intermediate gapless spin liquid phase, which has one gapless spin mode and algebraic spin–spin correlations but exponential decay scalar chiral–chiral correlations, between a metallic phase at weak coupling and Mott insulating dimer phase at strong interaction. Upon light doping the gapless spin liquid, the system exhibits power-law charge-density-wave (CDW) correlations but short-range single-particle, spin–spin, and chiral–chiral correlations. Similar to CDW correlations, the superconducting correlations also decay in power-law but oscillate in sign as a function of distance, which is consistent with the striped pair-density wave. When further doping the gapless spin liquid phase or doping the dimer order phase, another phase takes over, which has similar CDW correlations but all other correlations decay exponentially.

Since the discovery of high-T_c superconductivity [1], the theoretical investigation of quantum materials has attracted numerous attention. Enormous theoretical studies not only focus on elucidating the pairing mechanism in cuprates, but also aims to explore entangled quantum states in similar correlated materials. Beyond the description of traditional mean-field theory, these exotic states have extended our understanding of fundamental quantum science and hold the promise for potential application in functional materials. The pair density wave (PDW) and quantum spin liquid (QSL) are among the most important exotic sates. Motivated by recent experimental observations [2, 3]: signatures of PDW states has been observed via local Cooper pair tunneling and scanning tunneling microscopy in underdoped $Bi_2Sr_2CaCu_2O_{8+x}$ [4–6], as well as the dynamical inter-layer decoupling in $La_{1.875}Ba_{0.125}CuO_4$ [7, 8]; promising evidences of QSLs have been revealed in triangular materials κ-$(ET)_2Cu_2(CN)_3$ [9] and $EtMe_3Sb[Pd(dmit)_2]_2$ [10–14]. Both experimental advances motivate systematic investigation of these two exotic phases.

Due to the presence of multiple competing instabilities in correlated materials, as will be detailed below, the theoretical identification of these phases requires microscopic models and unbiased solutions. As a straightforward simplification of quantum chemistry, the single-band Hubbard model has been one of the central paradigms in the field of correlated materials [15]. Although with only two parameters, the Hubbard model is widely believed to contain the essential ingredients of high-temperature superconductivity [16–18] and other important phases in correlated materials [19–25]. Thus, the theoretical study of the PDW and QSL phases in the Hubbard model is particularly important. Phenomenologically, PDW is a special type of superconducting (SC) state in which Cooper pairs carry finite center-of-mass momentum and the order parameter varies periodically in space in such a way that its spatial average vanishes [3, 26, 27]. The first example of PDW is the Fulde–Ferrell–Larkin–Ovchinnikov state [28, 29], which arises in a conventional

s-wave superconductor with a finite spin polarization at the Fermi surface. Despite the well-established phenomenological theory of PDW, its microscopic models and realization are still open questions [30–35]. These include the 1D Kondo–Heisenberg model [30], the extended Hubbard–Heisenberg model on a two-leg ladder [31], and strong coupling limit of the Holstein–Hubbard model [34, 35]. Apart from these models with canonical interactions, PDW signatures were also observed in the t–J model with four-spin ring exchange interaction (in a four-leg triangular cylinder) [33], the extended Hubbard model with a staggered magnetic flux on a three-leg triangular lattice [32], and the t–J-like extension of the Kitaev model (in a three-leg honeycomb cylinder) [36]. In addition to the above, no evidence of the PDW state was ever found in the standard Hubbard model on systems that wider than a two-leg ladder.

On the other hand, the QSL has been the subject of considerable interest in the geometrically frustrated triangular lattice [37, 38]. Through the substantial theoretical studies using this lattice [26, 39–53], it has became a consensus that the half-filled Hubbard model exhibits QSL phase at intermediate interaction strength, separating the metallic and Mott insulating phase [26, 44–47, 52–58]. However, the nature of this QSL phase remains still under debate: distinct candidates, including the QSL with spinon Fermi surfaces [26, 46–49, 52, 59], Z_2 spin liquid [50, 51] and chiral spin liquid (CSL) that breaking time-reversal symmetry [57, 58], have been proposed theoretically. Debates also exist in unbiased numerical simulations obtained using the density-matrix renormalization group (DMRG) [52, 57–60], particularly between the gapless spin liquid (in 2D) [52] and the gapped CSL (in four- and six-leg cylinders) [57, 58, 60].

A natural question which may bring these two exotic phases together is the physics of a doped QSL. Intuitively, QSL can be viewed as an insulating phase with preformed electron pairs such that superconductivity may immediately emerge upon light doping [18, 61–66]. This idea was supported by recent large-scale DMRG studies, which demonstrated that nematic d-wave [67], and topological $d \pm \mathrm{i}d$-wave superconductivity [68], emerge from lightly-doped (time-reversal symmetric) QSL and CSL, respectively. Specifically for the doped Hubbard model on the triangular lattice, various SC states had been proposed [32, 69–71], however, were recently challenged by the DMRG simulation in both three- and four-leg cylinders [72].

In this paper, we address the above questions by studying the Hubbard model on three-leg triangular cylinders of length up to $L_x = 128$ using DMRG [73]. Due to both the accommodation of 2D characteristics and the feasibility of well-controlled DMRG simulations, the three-leg cylinder is a good starting point. Our main results are summarized in the ground state phase diagram in figure 1. At half-filling, an intermediate time-reversal symmetric QSL phase separates the metallic phase at weak coupling $U < U_{c1} = 7.0 \pm 0.5t$ and the Mott insulating dimer phase at strong coupling $U > U_{c2} = 12.0 \pm 0.5t$. Distinct from the gapped CSL on four- and six-leg cylinders [57, 60], we find that the QSL phase on three-leg cylinders is gapless and preserves the time-reversal symmetry. Upon light-doping, this gapless spin liquid evolves into a state consistent with that of the striped PDW [3]: both the SC and charge correlations decay as a power-law and oscillate in distance. While other correlations (single-particle, spin–spin, and scalar chiral–chiral) are all short-range, all these correlations are intertwined and mutually commensurate in terms of the wavevector. In contrast, a charge-density-wave (CDW) phase is identified when further doping the gapless spin liquid phase with $\delta \gtrsim 10\%$ or doping the dimer order phase.

1. Model and method

The single-band Hubbard model on the triangular lattice is defined by the Hamiltonian

$$H = -t\sum_{\langle ij\rangle\sigma}(\hat{c}^{\dagger}_{i,\sigma}\hat{c}_{j,\sigma} + \mathrm{h.c.}) + U\sum_{i}\hat{n}_{i,\uparrow}\hat{n}_{i,\downarrow}. \tag{1}$$

Here, $\hat{c}^{\dagger}_{i\sigma}$ ($\hat{c}_{i\sigma}$) is the electron creation (annihilation) operator with spin-$\sigma(\sigma = \uparrow, \downarrow)$ on site $i = (x_i, y_i)$, $\hat{n}_{i,\sigma} = \hat{c}^{\dagger}_{i\sigma}\hat{c}_{i\sigma}$ is the electron number operator. t denotes the electron hopping amplitude between the nearest-neighbor (NN) sites $\langle ij\rangle$, and U is the on-site Coulomb repulsion. The lattice geometry used in our simulations is depicted in the inset of figure 1, with open (periodic) boundary condition along the $\mathbf{e}_1(\mathbf{e}_2)$ direction. We focus on three-leg triangular cylinders with width $L_y = 3$ and length up to $L_x = 128$, where L_y and L_x are the number of sites along the $\mathbf{e}_2$ and $\mathbf{e}_1$ directions, respectively. The doped hole concentration is defined as $\delta = N_{\mathrm{h}}/N$, where $N = 3L_x$ is the total number of lattice sites and N_{h} is the number of doped holes. We set $t = 1$ as an energy unit and consider $6t \leqslant U \leqslant 18t$ in the present study. We perform up to 69 sweeps and keep up to $m = 25\,000$ number of states with a typical truncation error $\epsilon \sim 5 \times 10^{-7}$. Further details of the numerical simulation are provided in the supplemental materials (https://stacks.iop.org/NJP/23/123004/mmedia).

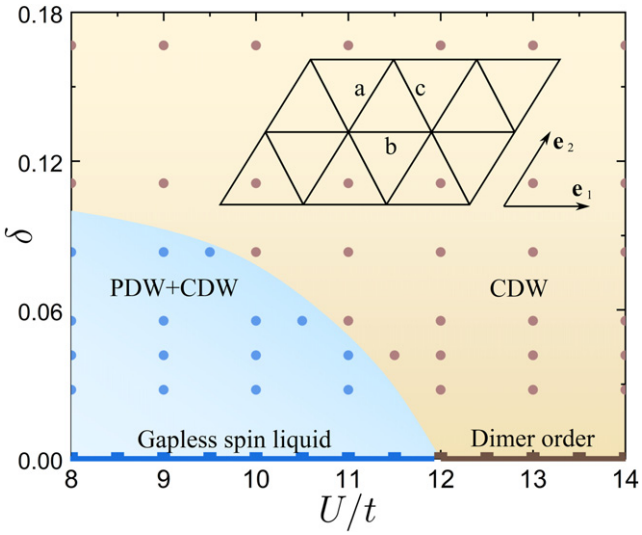

Figure 1. Ground state phase diagram of the Hubbard model in equation (1) on three-leg triangular cylinders as a function of U/t and hole doping concentration δ. The squares are data points for half-filling and the dots are data points at finite doping. Inset: the geometry of the triangular lattice where the two arrows labeled by $\mathbf{e}_1 = (1, 0)$ and $\mathbf{e}_2 = (1/2, \sqrt{3}/2)$ denote the two basis vectors. *a*, *b* and *c* label the three different bonds.

2. Gapless spin liquid

At half-filling, we identify three distinct phases (see figures 1 and 2) separated by two phase transitions at $U_{c1} = 7.0 \pm 0.5t$ and $U_{c2} = 12.0 \pm 0.5t$. These phases are determined by various energy gaps including the single-particle gap Δ_p, charge gap Δ_c and spin-triplet gap Δ_s defined as

$$\begin{aligned}\Delta_p &= E_{\frac{N}{2}+1,\frac{N}{2}} + E_{\frac{N}{2}-1,\frac{N}{2}} - 2E_{\frac{N}{2},\frac{N}{2}},\\ \Delta_c &= \left[E_{\frac{N}{2}+1,\frac{N}{2}+1} + E_{\frac{N}{2}-1,\frac{N}{2}-1} - 2E_{\frac{N}{2},\frac{N}{2}}\right]/2,\\ \Delta_s &= E_{\frac{N}{2}+1,\frac{N}{2}-1} - E_{\frac{N}{2},\frac{N}{2}}.\end{aligned} \tag{2}$$

Here $E_{N_\uparrow,N_\downarrow}$ is the ground state energy of the system with $N_\uparrow$ spin-up and $N_\downarrow$ spin-down electrons. Our calculations identify a metallic phase at $U < U_{c1}$ where all three gaps vanish in the thermodynamic limit, consistent with previous studies [47, 52, 56, 57]. At large $U > U_{c2}$, the ground state of the system can be mapped onto the spin-1/2 antiferromagnetic Heisenberg model. It has a dimerized ground state on three-leg cylinders [74] where all three gaps are expected to be finite in the thermodynamic limit. This is indeed consistent with our results as shown in figures 2(a)–(c) including the dimer pattern in the inset of figure 2(c). Independently, the phase boundaries can also be determined by $n_d U^2$, with the double occupancy $n_d = \frac{1}{N}\sum_i \langle \hat{n}_{i,\uparrow}\hat{n}_{i,\downarrow}\rangle$ [47], which exhibits peak and kink at the two phase boundaries (see figure 2(d)).

We focus on the intermediate phase among these three phases. Distinct with four- and six-leg cylinders, this intermediate phase on three-leg cylinders is consistent with a gapless spin liquid, where both Δ_p and Δ_c remain finite but Δ_s vanishes in the thermodynamic limit as shown in figures 2(a)–(c). To further support this, we consider $U = 10t$ as an example (deeply in the intermediate phase) and investigate the scaling behavior.

We first calculate the spin–spin correlation

$$F(r) = \frac{1}{L_y}\sum_{y=1}^{L_y} \langle \mathbf{S}_{(x_0,y)} \cdot \mathbf{S}_{(x_0+r,y)}\rangle, \tag{3}$$

where $\mathbf{S}_i$ is the $S = 1/2$ spin operator on site i and (x_0, y) is the reference site with $x_0 \sim L_x/4$ and r is the distance between two sites in the $\mathbf{e}_1$ direction. As shown in figure 3(a), it is clear that $F(r)$ decays with a power-law at long distances which can be well fitted by $F(r) \sim r^{-K_s}$ with corresponding Luttinger exponent $K_s = 1.1(1)$. As a further test, a key feature of the gapless spin liquid is its finite gapless spin mode characterized by the central charge *c*. It can be obtained from fitting the von Neumann entanglement entropy, $S(x) = -\mathrm{Tr}[\rho_x \ln \rho_x]$, through $S(x) = \frac{c}{6}\ln[\frac{L_x}{\pi}\sin(\frac{\pi x}{L_x})] + \mathrm{const}$, where ρ_x is the reduced density

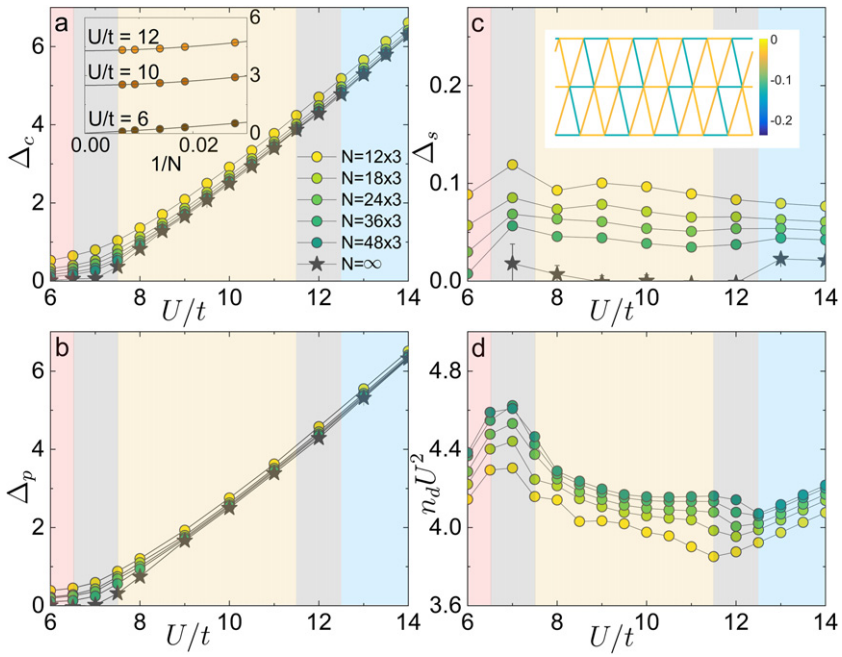

Figure 2. (a) Charge gap Δ_c, (b) single particle gap Δ_p, (c) spin gap Δ_s, and (d) double occupancy $n_d U^2$ as a function of U/t on three-leg triangular cylinders. The star symbols are extrapolated results in the limit $N \to \infty$. Insets: (a) examples of finite-size scaling of Δ_c at different U/t. (c) Dimer pattern, i.e. spin–spin correlation $\langle \mathbf{S}_i \cdot \mathbf{S}_j \rangle$ between NN sites $\langle ij \rangle$ at $U/t = 15$. The gray shaded regions denote the phase boundaries at U_{c1} and U_{c2}.

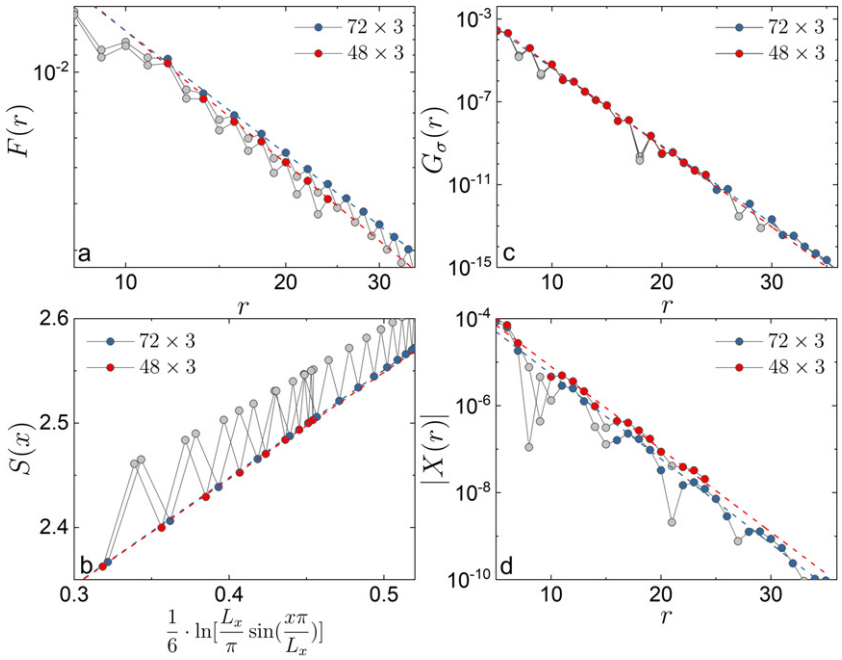

Figure 3. Correlation functions of the Hubbard model at half-filling with $U = 10t$. Data points far from the envelope are discarded in fittings and shown in gray color. (a) Spin–spin correlation $F(r)$ and its power-law fit $f(r) \sim r^{-K_s}$ labeled by the dashed lines. (b) von Neumann entanglement entropy $S(x)$ where the slope of the dashed lines gives the central charge c. (c) Single-particle correlation $G_\sigma(r)$ and its exponential fit $f(r) \sim e^{-r/\xi_G}$ labeled by the dashed lines. (d) Scalar chiral–chiral correlation $|X(r)|$ and its exponential fit $f(r) \sim e^{-r/\xi_X}$ labeled by the dashed lines.

matrix of a (quasi-) 1D subsystem with length x [75, 76]. For critical (quasi-) 1D systems, it has been established [75, 76] that $S(x) = \frac{c}{6} \ln[\frac{L_x}{\pi} \sin(\frac{\pi x}{L_x})] + \text{const}$. Examples are shown in figure 3(b) for cylinders of length $L_x = 48$ and $L_x = 72$, the extracted central charge is $c = 1.0(1)$ suggesting that the intermediate phase has one gapless mode.

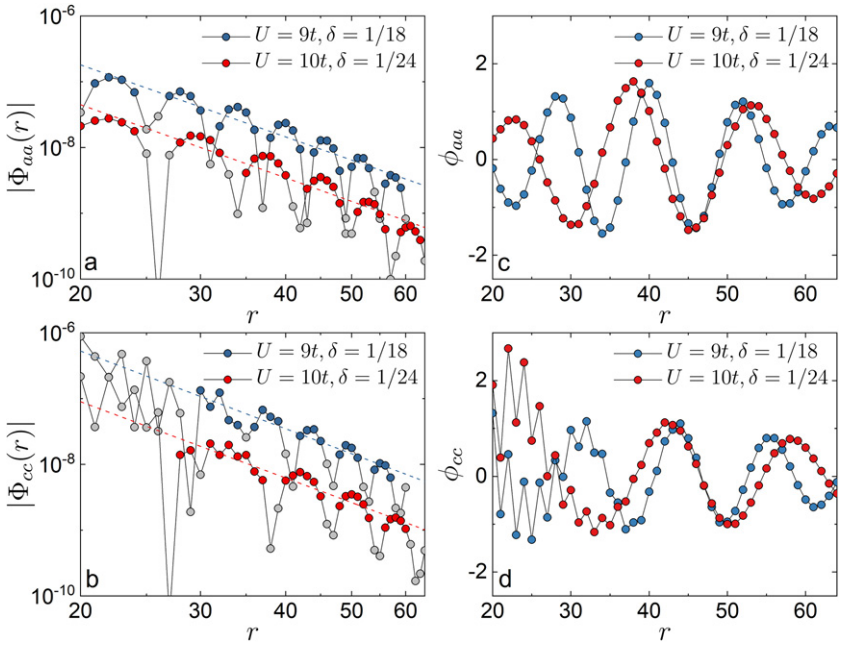

Figure 4. SC correlations (a) $|\Phi_{aa}(r)|$ and (b) $|\Phi_{cc}(r)|$ where dashed lines denote fittings to a power-law function $f(r) \sim r^{-K_{sc}}$. Data points far from the envelope as well as those at short distances without PDW signatures are discarded in the fitting process and shown in gray color. The normalized functions (c) $\phi_{aa}(r) = (-1)^r \Phi_{aa}(r)/f(r)$ and (d) $\phi_{cc}(r) = (-1)^r \Phi_{cc}(r)/f(r)$ reflect the spatial oscillation of $\Phi_{aa}(r)$ and $\Phi_{cc}(r)$, respectively.

In contrast to the spin channel, a finite single-particle gap in the intermediate phase suggests that the single-particle correlation

$$G_\sigma(r) = \frac{1}{L_y}\sum_{y=1}^{L_y} \langle c^\dagger_{(x_0,y),\sigma} c_{(x_0+r,y),\sigma}\rangle, \tag{4}$$

should decay exponentially as $G_\sigma(r) \sim e^{-r/\xi_G}$ with a correlation length ξ_G. This is indeed the case as shown in figure 3(c), where $G_\sigma(r)$ decays exponentially and the extracted correlation length is $\xi_G = 1.1(2)$.

To test the possibility of time-reversal symmetry breaking, we have also calculated the scalar chiral–chiral correlation $X(r)$, which is defined as

$$X(r) = \frac{1}{L_y}\sum_{y=1}^{L_y} \langle \chi_{(x_0,y)} \chi_{(x_0+r,y)}\rangle. \tag{5}$$

Here $\chi_i = \mathbf{S}_i \cdot (\mathbf{S}_j \times \mathbf{S}_k)$ is the scalar chiral operator, where i, j and k label clockwise vertices of a triangle. On three-leg cylinders, we find that $X(r)$ decays exponentially as $X(r) \sim e^{-r/\xi_\chi}$ at long distances with the correlation length $\xi_\chi = 2.2(1)$. Therefore, we conclude that the intermediate gapless spin liquid phase on three-leg cylinders preserves time-reversal symmetry, which is different from the gapped CSL on four- and six-leg cylinders in the previous study [57].

3. Lightly doped gapless spin liquid

Upon light doping the gapless spin liquid, a state which is consistent with that of the striped PDW emerges where the CDW and SC pair-field correlations decay spatially in a power-law at long distances. We provide two detailed examples ($U = 9t$, $\delta = 1/18$ and $U = 10t$, $\delta = 1/24$) in figure 4, while the conclusion holds for all parameter in the PDW + CDW phase of figure 1. In this paper, we have studied a sizable system with length up to $L_x = 128$ to suppress the finite-size effect. As shown below, the oscillation period of SC correlations is rather large, which results in the absence of the PDW correlation in previous study [72].

3.1. Pair density wave

To test the possibility of superconductivity, we calculate the equal-time SC pair-field correlations. As the ground state with an even number of electrons always have total spin 0, we focus on spin-singlet SC

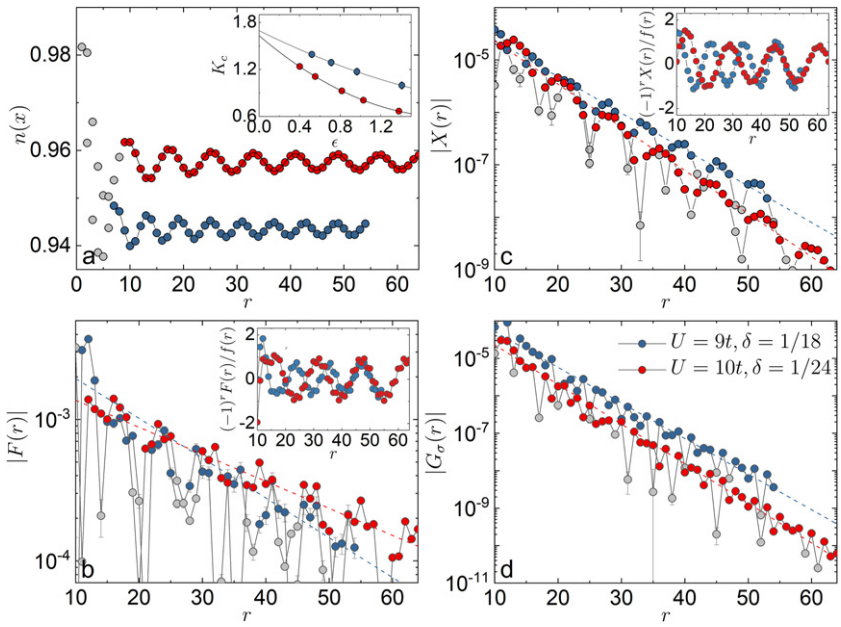

Figure 5. (a) Charge density profile $n(x)$ where the solid lines denote the fitting using equation (7). Data points in gray are discarded to minimize the boundary effect. Inset is the extracted exponent K_c as a function of truncation error ϵ. (b) Spin–spin correlation $F(r)$ and the exponential fitting $f(r) \sim e^{-r/\xi_S}$ (dashed lines). Inset: normalized correlation $(-1)^r F(r)/f(r)$. (c) Chiral–chiral correlation $|X(r)|$ and the exponential fitting $f(r) \sim e^{-r/\xi_X}$ (dashed lines). Inset: normalized correlation $(-1)^r X(r)/f(r)$. (d) Single-particle correlation $G_\sigma(r)$ and the exponential fitting $f(r) \sim e^{-r/\xi_G}$ labeled by the dashed lines. Note that data points far from the envelope or have large error bars are discarded in the fitting process and shown in gray color in (b)–(d).

correlation, which is defined as

$$\Phi_{\alpha\beta}(r) = \frac{1}{L_y}\sum_{y=1}^{L_y} \langle \Delta_\alpha^\dagger(x_0, y)\Delta_\beta(x_0 + r, y)\rangle. \tag{6}$$

Here, $\Delta_\alpha^\dagger(x,y) = \frac{1}{\sqrt{2}}[\hat{c}^\dagger_{(x,y),\uparrow}\hat{c}^\dagger_{(x,y)+\alpha,\downarrow} - \hat{c}^\dagger_{(x,y),\downarrow}\hat{c}^\dagger_{(x,y)+\alpha,\uparrow}]$ is spin-singlet pair creation operator living on bond $\alpha = a$, b and c (see figure 1 inset). (x_0, y) is the reference site with $x_0 \sim L_x/4$ and r is the distance between two bonds in the $\mathbf{e}_1$ direction. The spatial distribution of SC correlations $\Phi_{aa}(r)$ and $\Phi_{cc}(r)$ for the two examples are shown in figure 4: $\Phi(r)$ exhibits clear spatial oscillation which can be well fitted by $\Phi(r) \sim f(r)\phi(r)$ for a large region of r, where $f(r)$ sets envelope and $\phi(r)$ determines the oscillation, as discussed below. At long distances, the envelope function $f(r)$ is consistent with a power-law decay $f(r) \sim r^{-K_{sc}}$. The extracted exponent is $K_{sc} = 3.6(2)$ for $\Phi_{aa}(r)$ and $K_{sc} = 3.9(3)$ for $\Phi_{cc}(r)$, respectively. We have also calculated the spin-triplet SC correlations, which however are much weaker than the spin-singlet SC correlations.

The spatial oscillation of the SC correlations $\Phi(r)$ is characterized by the normalized function $\phi(r) = (-1)^r\Phi(r)/f(r)$ as mentioned above. Examples of $\phi_{aa}(r)$ and $\phi_{cc}(r)$ are shown in figures 4(c) and (d), both of which oscillate periodically in real space and can be well fitted by $\phi(r) \sim \sin(Qr + \theta)$ for $\phi_{aa}(r)$ when $r \gtrsim 8$ and $\phi_{cc}(r)$ when $r \gtrsim 24$. This is consistent with the striped PDW state with vanishing spatial average of $\phi(r)$. $Q = 3\pi\delta$ is the corresponding PDW ordering wavevector which corresponds to the wavelength $\lambda_{sc} = 2/3\delta$, i.e. $\lambda_{sc} = 12$ for $\delta = 1/18$ and $\lambda_{sc} = 16$ for $\delta = 1/24$. As we will see below, our results clearly show the relationship $\lambda_{sc} = \lambda_s = 2\lambda_c = \lambda_\chi$, which is expected for the striped PDW state. Here λ_s, λ_c and λ_χ are wavelengths of the spin–spin, CDW and scalar chiral–chiral correlations.

3.2. Charge density wave

To measure the charge order, we define the local rung density operator as $\hat{n}(x) = \sum_{y=1}^{L_y}\hat{n}(x, y)$ and its expectation value as $n(x) = \langle\hat{n}(x)\rangle$. Figure 5(a) shows the charge density profile $n(x)$ on cylinders of length $L_x = 108$ at $\delta = 1/18$ and $L_x = 128$ at $\delta = 1/24$. The system forms 1/3-filled charge stripes of wavelength $\lambda_c = 1/3\delta$, which is the spacing between two adjacent charge stripe along the cylinder. This corresponds to an ordering wavevector $K = 6\pi\delta = 2Q$ with 1/3 doped hole per CDW unit cell.

At long distances, the spatial decay of CDW correlations is dominated by a power-law with the Luttinger exponent K_c, which can be obtained by fitting the charge density oscillations (Friedel oscillations) induced

Table 1. Summary of the phases. Parameters, corresponding phases, exponents (K_s, K_c, K_{sc}), correlation lengths (ξ_s, ξ_G, ξ_χ) and central charge c. Note that K_c shown in the table is determined from the Friedel oscillation, and K_{sc} is extracted from SC correlation $\Phi_{aa(cc)}(r)$. The cylinder lengths and correlation lengths are in the unit of lattice spacing.

Parameters	Phase	K_s	ξ_s	ξ_G	ξ_χ	K_c	$K_{sc}(aa)$	$K_{sc}(cc)$	ξ_{sc}	c
$U = 10t, \delta = 0, L_x \leqslant 72$	Gapless QSL	1.1(1)	—	1.1(2)	2.2(1)	—	—	—	—	∼1
$U = 9t, \delta = 1/18, L_x \leqslant 108$	PDW + CDW	—	15(1)	4.5(1)	6.2(1)	1.6(1)	3.6(2)	3.9(3)	—	—
$U = 10t, \delta = 1/24, L_x \leqslant 128$	PDW + CDW	—	22(1)	4.1(1)	5.5(1)	1.6(1)	3.6(2)	3.9(3)	—	—
$U = 18t, \delta = 1/18, L_x \leqslant 72$	CDW	—	5.9(1)	10.8(5)	5.4(2)	1.6(1)	—	—	8.3(1)	∼1

by the boundaries of the cylinder [77, 78]

$$n(x) = n_0 + \delta n \cos(K * x + \theta) x^{-K_c/2}. \tag{7}$$

Here n_0 denotes the background electron density, δn and θ are model-dependent constants. Note that the first CDW period (figure 5(a), in gray), which is typically different from other CDW periods due to the boundary effect, has been excluded to minimize the boundary effect for a more reliable fitting. The extracted exponent $K_c = 1.6(1)$ is shown in the inset of figure 5(a). Alternatively, K_c can also be obtained from the charge density–density correlation, which gives consistent results (see supplemental materials for details).

3.3. Other correlations

To further characterize the PDW phase, we have also calculated other correlations including $F(r)$, $X(r)$ and $G_\sigma(r)$ as shown in figure 5. Contrary to CDW and SC correlations, we find that they decay exponentially at long distances as $F(r) \sim e^{-r/\xi_s}$, $X(r) \sim e^{-r/\xi_\chi}$ and $G_\sigma(r) \sim e^{-r/\xi_G}$, where the corresponding correlation lengths ξ_s, ξ_χ and ξ_G are given in table 1. It may be worth mentioning that while $F(r)$ decays exponentially at long distances, its correlation length is fairly long $\xi_s \sim 22(2)$. This can be attributed to the fact that the lightly doped case is very close to the gapless spin liquid at half-filling, which has divergent correlation length. Interestingly, we find that both $F(r)$ and $X(r)$ exhibit clear spatial oscillation as shown in the insets of figures 5(b) and (c) with wavelengths λ_s and λ_χ that are the same as that of the SC correlation, i.e. $\lambda_s = \lambda_\chi = \lambda_{sc}$. This gives the same ordering wavevector Q as the SC correlation. These features further support the striped PDW state in the lightly doped system.

4. Conclusion

In summary, we have studied the ground state properties of the Hubbard model on sizable three-leg triangular cylinders. Based on our results, we conclude that the exact ground state of the system has the following properties: (1) at half-filling, there is an intermediate gapless spin liquid phase which is characterized by one gapless spin mode and power-law spin–spin correlation but a gap to all charge excitations. (2) Light doping ($\delta \lesssim 10\%$) the gapless spin liquid phase can give rise to a striped PDW state with power-law SC correlations with moderate exponent $K_{sc} \sim 4$ and an ordering wavevector Q. (3) There are power-law CDW correlations with an ordering wavevector $K = 2Q$. (4) While both spin–spin and scalar chiral–chiral correlations are short-ranged, they are mutually commensurate with both CDW and SC correlations with an ordering wavevector Q. It is notable that the favored forms of order, where stripe spin density wave and SC correlations with the same ordering wavevector Q is half of the ordering wavevector $K = 2Q$ of the CDW, are remarkably reminiscent of those conjectured to be present in the cuprate high-temperature superconductor [4–8]. In this paper, we primarily focus on the single-band Hubbard mode, and observe the evidence of the power-law PDW correlation on the triangular lattice wider than the two-leg ladder. The present results are suggestive of a possible PDW ordered state for doping the QSL on triangular materials such as κ-$(ET)_2Cu_2(CN)_3$ [9] and $EtMe_3Sb[Pd(dmit)_2]_2$ [10–14].

Acknowledgments

We would like to thank Thomas Devereaux and especially Steve Kivelson for insightful discussion and invaluable suggestions. This work was supported by the Department of Energy, Office of Science, Basic Energy Sciences, Materials Sciences and Engineering Division, under contract DE-AC02-76SF00515. YW acknowledges support from National Science Foundation (NSF) award DMR-2038011. Parts of the

computing for this project was performed on the Sherlock cluster. Parts of the calculations in figures 1 and 2 are performed using the high-performance matrix product state algorithm library GraceQ/tensor [79].

Data availability statement

All data that support the findings of this study are included within the article (and any supplementary files).

ORCID iDs

Cheng Peng https://orcid.org/0000-0002-9267-1789
Hong-Chen Jiang https://orcid.org/0000-0003-2842-6591

References

[1] Bednorz J G and Müller K A 1986 *Z. Phys.* B **64** 189
[2] Senthil T 2008 *Phys. Rev.* B **78** 045109
[3] Agterberg D F *et al* 2020 *Annu. Rev. Condens. Matter Phys.* **11** 231
[4] Hamidian M H *et al* 2016 *Nature* **532** 343
[5] Ruan W, Li X, Hu C, Hao Z, Li H, Cai P, Zhou X, Lee D-H and Wang Y 2018 *Nat. Phys.* **14** 1178
[6] Edkins S D *et al* 2019 *Science* **364** 976
[7] Li Q, Hücker M, Gu G D, Tsvelik A M and Tranquada J M 2007 *Phys. Rev. Lett.* **99** 067001
[8] Tranquada J M *et al* 2008 *Phys. Rev.* B **78** 174529
[9] Shimizu Y, Miyagawa K, Kanoda K, Maesato M and Saito G 2003 *Phys. Rev. Lett.* **91** 107001
[10] Itou T, Oyamada A, Maegawa S, Tamura M and Kato R 2007 *J. Phys.: Condens. Matter* **19** 145247
[11] Itou T, Oyamada A, Maegawa S, Tamura M and Kato R 2008 *Phys. Rev.* B **77** 104413
[12] Itou T, Oyamada A, Maegawa S and Kato R 2010 *Nat. Phys.* **6** 673–6
[13] Yamashita M, Nakata N, Senshu Y, Nagata M, Yamamoto H M, Kato R, Shibauchi T and Matsuda Y 2010 *Science* **328** 1246
[14] Yamashita S, Yamamoto T, Nakazawa Y, Tamura M and Kato R 2011 *Nat. Commun.* **2** 275
[15] Zhang F C and Rice T M 1988 *Phys. Rev.* B **37** 3759
[16] Dagotto E 1994 *Rev. Mod. Phys.* **66** 763
[17] Lee P A, Nagaosa N and Wen X-G 2006 *Rev. Mod. Phys.* **78** 17
[18] Fradkin E, Kivelson S A and Tranquada J M 2015 *Rev. Mod. Phys.* **87** 457
[19] Zheng B-X *et al* 2017 *Science* **358** 1155
[20] Huang E W, Mendl C B, Liu S, Johnston S, Jiang H-C, Moritz B and Devereaux T P 2017 *Science* **358** 1161
[21] Huang E W, Mendl C B, Jiang H-C, Moritz B and Devereaux T P 2018 *npj Quantum Mater.* **3** 22
[22] Ponsioen B, Chung S S and Corboz P 2019 *Phys. Rev.* B **100** 195141
[23] Kokalj J 2017 *Phys. Rev.* B **95** 041110
[24] Huang E W, Sheppard R, Moritz B and Devereaux T P 2019 *Science* **366** 987
[25] Cha P, Patel A A, Gull E and Kim E-A 2020 *Phys. Rev. Res.* **2** 033434
[26] Lee S-S and Lee P A 2005 *Phys. Rev. Lett.* **95** 036403
[27] Lee P A 2014 *Phys. Rev.* X **4** 031017
[28] Fulde P and Ferrell R A 1964 *Phys. Rev.* **135** A550
[29] Larkin A I and Ovchinnikov Y N 1965 *Soviet Physics-JETP* **20** 762–70 https://elibrary.ru/item.asp?id=21823687
[30] Berg E, Fradkin E and Kivelson S A 2010 *Phys. Rev. Lett.* **105** 146403
[31] Jaefari A and Fradkin E 2012 *Phys. Rev.* B **85** 035104
[32] Venderley J and Kim E-A 2019 *Phys. Rev.* B **100** 060506
[33] Xu X Y, Law K T and Lee P A 2019 *Phys. Rev. Lett.* **122** 167001
[34] Han Z, Kivelson S A and Yao H 2020 *Phys. Rev. Lett.* **125** 167001
[35] Huang K S, Han Z, Kivelson S A and Yao H 2021 arXiv:2103.04984
[36] Peng C, Jiang Y-F, Devereaux T P and Jiang H-C 2021 *npj Quantum Mater.* **6** 64
[37] Anderson P W 1973 *Mater. Res. Bull.* **8** 153
[38] Balents L 2010 *Nature* **464** 199–208
[39] Misguich G, Lhuillier C, Bernu B and Waldtmann C 1999 *Phys. Rev.* B **60** 1064
[40] LiMing W, Misguich G, Sindzingre P and Lhuillier C 2000 *Phys. Rev.* B **62** 6372
[41] Mishmash R V, Garrison J R, Bieri S and Xu C 2013 *Phys. Rev. Lett.* **111** 157203
[42] Kyung B and Tremblay A-M S 2006 *Phys. Rev. Lett.* **97** 046402
[43] Clay R T, Li H and Mazumdar S 2008 *Phys. Rev. Lett.* **101** 166403
[44] Morita H, Watanabe S and Imada M 2002 *J. Phys. Soc. Japan* **71** 2109
[45] Koretsune T, Motome Y and Furusaki A 2007 *J. Phys. Soc. Japan* **76** 074719
[46] Motrunich O I 2005 *Phys. Rev.* B **72** 045105
[47] Yang H-Y, Läuchli A M, Mila F and Schmidt K P 2010 *Phys. Rev. Lett.* **105** 267204
[48] Sheng D N, Motrunich O I and Fisher M P A 2009 *Phys. Rev.* B **79** 205112
[49] Block M S, Sheng D N, Motrunich O I and Fisher M P A 2011 *Phys. Rev. Lett.* **106** 157202
[50] Hu W-J, Gong S-S, Zhu W and Sheng D N 2015 *Phys. Rev.* B **92** 140403
[51] Qi Y and Sachdev S 2008 *Phys. Rev.* B **77** 165112
[52] Shirakawa T, Tohyama T, Kokalj J, Sota S and Yunoki S 2017 *Phys. Rev.* B **96** 205130
[53] Sahebsara P and Sénéchal D 2008 *Phys. Rev. Lett.* **100** 136402
[54] Laubach M, Thomale R, Platt C, Hanke W and Li G 2015 *Phys. Rev.* B **91** 245125

[55] Yoshioka T, Koga A and Kawakami N 2009 *Phys. Rev. Lett.* **103** 036401
[56] Mizusaki T and Imada M 2006 *Phys. Rev.* B **74** 014421
[57] Szasz A, Motruk J, Zaletel M P and Moore J E 2020 *Phys. Rev.* X **10** 021042
[58] Szasz A and Motruk J 2021 (arXiv:2101.07454 [cond-mat.str-el])
[59] Mishmash R V, González I, Melko R G, Motrunich O I and Fisher M P A 2015 *Phys. Rev.* B **91** 235140
[60] Chen B-B, Chen Z, Gong S-S, Sheng D N, Li W and Weichselbaum A 2021 (arXiv:2102.05560)
[61] Anderson P W 1987 *Science* **235** 1196
[62] Kivelson S A, Rokhsar D S and Sethna J P 1987 *Phys. Rev.* B **35** 8865
[63] Rokhsar D S and Kivelson S A 1988 *Phys. Rev. Lett.* **61** 2376
[64] Laughlin R B 1988 *Science* **242** 525
[65] Wen X G, Wilczek F and Zee A 1989 *Phys. Rev.* B **39** 11413
[66] Broholm C, Cava R J, Kivelson S A, Nocera D G, Norman M R and Senthil T 2020 *Science* **367** eaay0668
[67] Jiang H-C 2021 *npj Quantum Mater.* **6** 71
[68] Jiang Y-F and Jiang H-C 2020 *Phys. Rev. Lett.* **125** 157002
[69] Raghu S, Kivelson S A and Scalapino D J 2010 *Phys. Rev.* B **81** 224505
[70] Chen K S, Meng Z Y, Yu U, Yang S, Jarrell M and Moreno J 2013 *Phys. Rev.* B **88** 041103
[71] Guo H, Zhu X, Feng S and Scalettar R T 2018 *Phys. Rev.* B **97** 235453
[72] Zhu Z, Sheng D N and Vishwanath A 2020 (arXiv:2007.11963)
[73] White S R 1992 *Phys. Rev. Lett.* **69** 2863
[74] Chen R, Ju H, Jiang H-C, Starykh O A and Balents L 2013 *Phys. Rev.* B **87** 165123
[75] Calabrese P and Cardy J 2004 *J. Stat. Mech.* p06002
[76] Fagotti M and Calabrese P 2011 *J. Stat. Mech.* p01017
[77] White S R, Affleck I and Scalapino D J 2002 *Phys. Rev.* B **65** 165122
[78] Moreno A, Muramatsu A and Manmana S R 2011 *Phys. Rev.* B **83** 205113
[79] Grace Quantum GraceQ/tensor: A high-performance tensor computation framework for the quantum physics community http://GraceQuantum.org